PSFC/JA-06-14

RF-Plasma Edge Interactions and Their Impact on ICRF Antenna Performance in Alcator C-Mod

S.J. Wukitch, Y. Lin, T. Graves, A. Parisot and the C-Mod Team

MIT Plasma Science and Fusion Center, Cambridge, MA 02139 USA.

Plasma Science and Fusion Center
Massachusetts Institute of Technology
Cambridge MA 02139 USA

This work was supported by the U.S. Department of Energy, Grant No. DE-FC02-99ER54512. Reproduction, translation, publication, use and disposal, in whole or in part, by or for the United States government is permitted.

RF Plasma Edge Interactions and Their Impact on ICRF Antenna Performance in Alcator C-Mod

S.J. Wukitch,* B. Lipschultz, E. Marmar, Y. Lin, A. Parisot, M. Reinke, J. Rice, J. Terry, and the C-Mod Team

MIT Plasma Science and Fusion Center, Cambridge, MA 02139, USA

Abstract

In Alcator C-Mod, we have investigated the compatibility of high power ion cyclotron range of frequencies antenna with high performance plasmas and all high-Z plasma facing components, to provide operational information for future devices such as ITER. Boronization appears to be critical achieving low radiated power plasmas and is eroded rapidly such that the best performance is lost when the integrated injected RF energy reaches ~50 MJ. Since Ohmic H-modes with similar integrated input energy show a significantly slower degradation, an RF erosion mechanism is playing a significant role. RF-enhanced sheaths on flux tubes connected from the antennas to the top of the outer divertor are the most likely erosion mechanism. Antenna operation without a Faraday screen was found to degrade antenna performance through increased impurity sources.

JNM keywords: Impurities, Plasma-materials interaction
PSI-17 keywords: Alcator C-Mod, ICRF, RF, Sheaths
PACS: 52.40.Fd, 52.40.Hf, 52.40.Kh, 52.40.Qt
**Corresponding author address:* MIT Plasma Science and Fusion Center, NW21-103, 190 Albany St. Cambridge, MA 02139
**Corresponding author e-mail:* wukitch@mit.edu
Presenting author: Stephen J Wukitch

1. Introduction

Ion cyclotron range of frequency (ICRF) power is anticipated to be a primary auxiliary heating source in next step tokamak experiments like ITER.[1] The issues associated with ICRF utilization can be roughly divided into propagation and absorption (heating efficiency) and plasma surface interactions (compatibility), particularly at the antenna. With respect to plasma surface interactions, one can group compatibility issues as follows: a) How the scrape of layer (SOL) affects the antenna performance; and b) how antenna operation affects the core plasma performance and plasma facing components (PFCs).

Alcator C-Mod has developed a set of experimental tools and capabilities that enable unique ICRF compatibility studies. C-Mod high-Z (molybdenum) PFCs provide information for comparison to most other tokamaks which utilize carbon PFCs. In addition, operational experience with molybdenum PFCs is useful for predicting reactor situations where, at the moment, tungsten is the generally accepted PFC material. The use of electron cyclotron (EC) resonance discharges for application of the boronization coating allows the B deposition to be applied over small ranges of major radius as opposed to more typical glow discharge. Since the PFC surfaces are molybdenum the boron coatings can be removed more readily than carbon PFCs. The localized nature of the boronization affords an opportunities identify whether the boron coating must cover all PFCs, localize where the B coating is most effective, and characterize its lifetime. Further, we have a flexible ICRF system featuring two antennas allowing comparisons between antennas using one as a control.

A challenging requirement for ICRF antennas is the ability to reliably deliver RF waves to the plasma at high power density (>10 MW/m^2). Problems that arise include impurity generation, density influx, and voltage breakdown. This has been an active area of research on all machines utilizing ICRF including ASDEX-U, DIII-D, JET, JT-60, TEXTOR,

TFTR, and Tore Supra. Presently we lack a comprehensive antenna plasma model that can properly predict the antenna operational characteristics using antenna geometry, plasma density and temperature profiles, and taking into account the myriad possible physics phenomena associated with RF plasma edge interactions[2]. In this paper we concentrate on impurity generation and erosion of boron coatings.

A generally accepted model for ICRF induced impurity production is enhanced sputtering caused by RF sheaths with substantially higher sheath voltages (~500 V) than expected for thermal sheaths (~$3T_e$).[3] These enhanced sheaths form as a result of electrostatic, electromotive and electromagnetic mechanisms, and are both local to antenna elements and to far-field locations such as plasma limiters and divertor tiles.[4] A simple description of RF sheaths is as follows: An open field line with its ends terminating on conducting surfaces encloses an area where RF flux changes lead to voltage changes on this field line at the RF frequency. Since the electrons are much more mobile, electrons are preferentially lost to conducting surfaces. To maintain ambipolarity the sheath potential rises to inhibit electron losses. This enhanced sheath potential is essentially DC, leading to the term sheath-rectification. Because sheath rectification can be a strong effect, it is to determine where the primary impurity source is located. In JET, the antenna Faraday screens were identified as their primary source of impurities during RF.[5] In C-Mod, the Mo generated at the antenna has been shown to track the central Mo content[6] and motivated an experiment to replace the Mo tiles with BN tiles.

In addition to impurity production, sheath rectification is thought to underlie many RF edge plasma phenomena.[3] Among the more important is convective cell formation resulting in asymmetric plasma heating of antenna structure.[7,8,9] As a result of a radial gradient in the RF fields, the open field lines nearest the antenna charge more positively than others. The resultant radial E-field creates an ExB drift convecting plasma, creating an

asymmetry in the heat load to the antenna.[10] This mechanism has been proposed to explain a number of experimental observations where the density on field lines connected to or passing near the antenna decreases.[11,12,13,14] Recent theoretical work suggests the sheath can also interact directly with plasma filaments (blobs) and result in increased radial transport.[3,15] This mechanism could perhaps explain the observation from TEXTOR that the SOL density decay length was up to a factor of 4 longer for ICRF heated than neutral beam heated plasmas[16] and similar observations were made on JET.[17]

A typical ICRF antenna consists of the current straps housed in an antenna box with a Faraday screen between the straps and the plasma. The entire antenna structure is often protected by tiles mounted on the outside edges (toroidally and poloidally) of the antenna box. The use of Faraday screens dates back to the mid-1960s where a Faraday screen was placed on the outside of the alumina section of the race track vacuum vessel under the RF antenna on the Model-C Stellarator.[18] The logic was to eliminate electric fields along the confining magnetic field so as to prevent space charge build up resulting from the preferential loss of electrons. The space charge then accelerated ions into the ceramic surface resulting in sputtering of impurity ions. The installation of the Faraday shield on the C Stellerator resulted in a dramatically improved stored energy, reduced impurity influx, and led to agreement between experimental and theoretical antenna loading.

In tokamaks, Faraday screens have become standard plasma facing antenna components despite being an impurity source[5]. In contrast, a shield-less antenna would have reduced RF losses and simpler antenna design. Operation without a screen has had mixed results. JET results were interpreted as confirming that a screen is necessary, and the elements had to be aligned with the B-field[19] and be coated with low Z material[20]. TEXTOR demonstrated good performance in L-mode and I-mode without a Faraday screen [21,22] and Phaedrus-T showed significant antenna performance improvement with the

shield removed.[23] ASDEX-U reported that the shield-less antenna had lower heating effectiveness than shielded antennas.[24] DIII-D found degraded voltage handling, increased impurity production, and lower heating effectiveness for screen-less operation.[25] If a screen is necessary, another issue is whether the screen elements need to be aligned with the total field. This too has conflicting experimental results with JET results indicating that shields need to be aligned and TFTR, DIII-D, and C-Mod indicating no difference. The sensitivity to screen alignment to the B-field could be dependent on the relative importance of impurity sources in different machines.

In this paper, we report on the progress identifying the RF mechanism responsible for, and location of, the boronization erosion and subsequent impurity production. Second, we present results comparing antenna operation with and without a Faraday screen.

2. Experimental Description

Alcator C-Mod is a compact (major radius R = 0.67 m, minor radius a = 0.22 m), high field ($B_T \leq 8.1$ T) diverted tokamak[26]. The discharges analyzed here are so-called fiducial discharges: lower single-null D discharges, H-minority heated, on-axis toroidal fields, B_T, were 5.2-5.4 T, the plasma current, I_p, was 1 MA, and target central density $\leq 2 \times 10^{20}$ m^{-3}. For these experiments, 2-3 MW of ICRF is coupled to the plasma with the H cyclotron resonance near the magnetic axis. The minority concentration is typically 3-5% and the single pass absorption is strong (>80%), similar to that expected for ITER. The ICRF heating power is coupled to the plasma via three fast wave antennas, see Figure 1. The two-strap antennas, D and E,[27] are operated in dipole $(0,\pi)$ phasing, at 80 and 80.5 MHz, respectively and the four-strap antenna, J,[28] is operated at 78 MHz in dipole phase $(0,\pi,0,\pi)$.

The primary plasma diagnostics are the stored plasma energy (W_{MHD}) derived from EFIT [29] and impurity diagnostics. Bolometry is used to monitor plasma radiation [30,31,32] and spectroscopic measurements are utilized to monitor specific impurity species,

for example Mo and Cu.[33] The Mo and Cu densities are inferred using the measured line brightnesses, Thomson scattering electron density and temperature profiles, the MIST impurity transport code [34], transport coefficients [35] and cooling curves [36,37,38].

C-Mod utilizes a boronization process that coats all PFCs with a thin layer of B and results in enhances plasma performance characterized by increased energy confinement time and reduced impurity and radiative losses.[39] The boronization procedure used in these experiments utilizes a helium diborane mixture (20% B_2D_6, 80% He) as the working gas, 2-3 kW of 2.45 GHz source, and a field to place the electron cyclotron in the chamber to create the plasma discharge. To enhance toroidal uniformity, the diborane is injected into the chamber through a single tube that splits into two, half turn toroidal tubes with holes spaced ~1 cm. A thin boronization layer can also be applied between full tokamak discharges (10-15 nm) and is typically eroded by one RF heated discharge. For the experiments described herein, the between-discharge boronization (BDB) is performed by sweeping the ECDC resonance location between 0.65 m and .75 m for 10 minutes.

3. Identification of Primary RF Impurity Source and Boronization Erosion

In C-Mod, there is a clear correlation between high performance (high confinement) H-modes and low impurity radiation.[33] Molybdenum radiation is the dominant contributor to the radiated power; therefore, limiting the impurity (Mo) influx is important, particularly during the formation stage of the H-mode. The impurity influx can be temporarily controlled through boronization. In C-Mod, we find that after ~ 20 ICRF-heated discharges, integrated injected ICRF energy is ~50 MJ, the Mo levels have risen and the confinement degrades.[33] From post campaign inspections, the B layer is still present everywhere except for a few regions. The largest area of B erosion is near the outer divertor strike point (point 'D' in Figure 2) [40]. Other smaller eroded areas are the upper gusset tiles (Figure 2, 'A'), leading

tile edges on the top of the outer divertor (Figure 2, 'C'), and limiters (Figure 2, 'B'). This suggests the B is being eroded from key locations resulting in degraded H-mode performance. The localized nature of the boron erosion is supported by an improvement in radiated power in the target L-mode plasma when the boronization discharge resonance was centered on 0.7 m.[33] This corresponds to the top of the outer divertor and upper gusset tiles (see Figure 2). This suggests that impurity sources outside the divertor are important in determining the core radiated power. Finally, we have also observed that the effect from a single BDB is significantly longer for Ohmic H-mode discharges in comparison with RF heated H-mode discharges.[41] This suggests RF is enhancing the erosion rate of the B layer.

To identify the importance of the antenna and plasma limiters as sources of core Mo, we replaced the side tiles with insulating BN tiles.[42] This should have eliminated sheath effects on field lines connected to the antenna. Surprisingly, the plasma performance and core Mo content were unimproved. This suggests antenna and limiter Mo sources are secondary compared with some other source.

To identify potential RF related Mo sources, we have mapped magnetic flux tubes from various parts of the antennas to PFC surfaces around the vessel. The flux tubes can be grouped into three categories: 1) flux tubes that pass in front of the antenna between the separatrix and the main limiter radius; 2) flux tubes on flux surfaces between the limiter radius and the antenna limiter radius (0.5 cm difference) and; 3) flux tubes that intersect the sides of the antennas. Those flux tubes in classes 2 and 3 connect to either the main limiters, upper gusset tiles, or the top of the outer divertor. Group one map to some of the same gusset tiles as well as the inner divertor and the top of the outer divertor nearest the plasma X-point. Shown in Figure 1 and Figure 2 are the toroidal and poloidal projections of field lines passing in front of both D+E and J antennas. Note that although the flux tubes for both antennas terminate on top of the outer divertor and upper gusset tiles, they intersect those surfaces at

different toroidal locations. This mapping has several implications. First, class 1 & 2 flux tubes that pass in front of the antenna connect between the upper/inner divertor and lower divertor. Sheath potentials on such field lines would be relatively unaffected by installing insulating limiters on the antennas. Second, field lines ending on the top of the outer divertor are in the approximate region where the BDB was most effective at controlling radiated power. Finally, the erosion caused by one antenna (D or E) is likely occurring at different locations than for the other antenna (J).

To test the above model, a series of discharges were run where the first discharge following a BDB was heated by one antenna or another (in this case D+E are utilized as one antenna) followed by a second discharge using a different antenna (without additional BDB). We already know if this is done with the same antenna that the plasma performance degrades substantially for the second discharge. An example of such a discharge sequence is shown in Figure 3 where the discharge is first heated by the D+E antenna combination followed by a discharge heated by the J antenna alone.

Interestingly, the antennas have different boron erosion rates. The degradation in performance (which we link to erosion of the boronization) was slower for the J antenna compared to D+E antennas as shown in Figure 4 where the stored energy degradation and radiated power increase is slower for the J antenna than for D+E antenna. There are a number of interpretations consistent with this observation due to the imprecise nature of the experiment: One possibility is that the boronization is toroidally non-uniform despite the efforts to ensure it is. Another possibility is that the local impurity production is higher on the D+E antenna limiter tiles. Cameras monitoring D and J antenna clearly show stronger interaction on the D antenna compared to J antenna but this is difficult to quantify. Finally, D and E antennas are operated at 80.5 and 80 MHz respectively; therefore, the D+E antenna symmetry is lost resulting larger RF sheaths for D+E compared to the J antenna.

Finally, an IR camera monitors the top of the divertor (location 'C' in Figure 2) at one toroidal location (between 'J' and 'K' ports) which maps to the D & E antennas. Simultaneous spectroscopic measurements of the Mo influx rate are made of the top of the divertor mapping to the D+E antenna. During the period when the D/E antennas are powered, a small temperature rise (~50 ^{o}C) is observed on top of the divertor whereas elsewhere on the divertor the no temperature rise is observed. The local correlation of the surface temperature rise and the increased Mo influx rate suggest the RF enhanced erosion is a result of non-thermal ion sputtering.

4. Role of Faraday Screen

To study the compatibility of screen-less ICRF antenna operation with high performance plasmas, the Faraday screen was removed from the J antenna and simple Mo septa were installed between each of the 4 antenna straps to prevent direct interaction between the strap and plasma, see Figure 5. These septa have toroidally-running slots to minimize the effect on the launched antenna spectrum. The septa are ~1 cm wide and the slot height is set to prevent particles from streaming into the antenna along field lines. Previously, when all C-Mod antennas were operated with Faraday screens, we demonstrated that all antennas had similar heating effectiveness[42]. Once the J antenna Faraday screen was removed we repeated the comparison. The J antenna (screen-less) voltage and power handling were unchanged compared to operation with a screen (35 kV and 3 MW were achieved). The loading was also very similar to previous operation and no enhanced loading at low power levels, as low as 10 kW, is observed suggesting no significant plasma in the antenna box.[43,44] We found the J antenna heating effectiveness, however, was ~10% and 15-20% less than D and E antennas in L-mode and H-mode plasmas, respectively. A comparison of two H-modes is shown in Figure 6. The degradation of J antenna performance was independent of plasma current and the magnitude of gap between separatrix and the outer

limiter. Shown in Figure 7 is the relative Cu density in the core plasma as a function of the input power for the different antennas. It shows a strong correlation with J antenna operation and power level that was previously not present with operation with a Faraday screen in prior campaigns.

The degradation of performance in both L- and H-mode plasmas can be largely attributed to the influx of Cu with RF power. The Cu influx has both direct and indirect consequences: First, the Cu contribution to overall radiated power is ~30% of the injected RF power thus effectively decreasing the heating. Second, the Cu line emission will be concentrated in the pedestal region potentially lowering the edge temperature pedestal and overall confinement. To improve screen-less operation, a reduction in the Cu influx with RF is required. The bridge region of the strap which we infer above to be the primary source of Cu, is also where one would expect a strong sheath effect. Common to all screen-less antenna experiments that experienced decreased performance are uncovered radial elements that provide significant RF field components other than the desired: C-Mod antenna bridge section; DIII-D radial feeds; the ASDEX-U bridge section. In those experiments where screen-less antenna operation worked or even improved antenna performance such elements were covered and sheaths further eliminated by using insulating limiters. Thus perhaps a key issue for antenna design is the minimization of B_r (radial) and B_θ (poloidal). In the event an antenna does have some of these fields, a Faraday screen will minimize or prevent direct antenna strap – plasma interactions.

5. Summary

We have identified RF sheaths as the primary culprit for significant core Mo and boronization erosion in C-Mod. The most important source/erosion location is on the top of the outer divertor.

In its present configuration, the J antenna is incompatible with screen-less operation due to excessive impurity production local to the antenna. In general, the problem may have less to do with the screen function than the antenna design which in this case has potential for strong sheath formation near the middle of the current strap.

Acknowledgements

We greatly appreciate the efforts of the entire Alcator C-Mod physics and operational staff. This work is supported by U.S. Department of Energy Coop. Agreement DE-FC02-99ER54512.

References

[1] ITER Physics Expert Group, Nuclear Fusion **39**, (1999) 2495.
[2] J.M. Noterdaeme and G. Van Oost, Plasma Phys. Control. Fusion **11** (1993) 1481.
[3] J. Myra, 16th Topical Conference on RF Power in Plasmas, AIP Conference Proceedings **787** (2006) 3.
[4] C.E. Harris et al., Fusion Tech. **30** (1996) 1.
[5] M. Bures et al., Plasma Physics Control. Fusion **33** (1991) 937.
[6] B. Lipschultz, et al., Nuclear Fusion **41** (2001) 585.
[7] D'Ippolito, J.R. Myra, J. Jacquinot and M. Bures, Phys. Fluids B **5** (1993) 3603.
[8] L. Colas et al., Nuclear Fusion **43** (2003) 1.
[9] L. Colas, S. Heuraux, S. Bremond and G. Bosia, Nuclear Fusion **45** (2005) 767.
[10] L. Colas, E. Faudot, S. Bremond and S. Heuraux, Topical Conference on RF Power in Plasmas, AIP Conference Proceedings **787** (2006).
[11] T. Tanaka, R. Majeski, D. Diebold, and N. Hershkowitz, Nuclear Fusion **36** (1996) 1609.
[12] J.-M. Noterdaeme et al., Proc. 23th IPS conf. on Control. Fusion and Plasma Physics (Kiev, Ukraine) **20** (1997) 723.
[13] D.A. D'Ippolito et al., Nuclear Fusion **42** (2002) 1357.
[14] A. Ekedahl et al., Proc 15th Topoical Conf. on Radio Frequency Power in Plasmas, AIP Conference Proceedings **694** (2003) 259.
[15] D.A. D'Ippolito, J.R. Myra, D.A. Russell and M.D. Carter, 16th Topical Conference on RF Power in Plasmas, AIP Conference Proceedings **787** (2006).
[16] D. Bora, G. Van Oost, and U. Samm, Nuclear Fusion **31** (1991) 2383.
[17] J. A. Tagle et al., J. Nuclear Material **196-198** (1992) 409.
[18] S. Yoshikawa, M. A. Rothman, and R. M. Sinclair, Phys. Rev. Lett. **14**, (1965) 214.
[19] M. Bures et al., Nucl. Fusion **30** (1990) 251.
[20] M. Bures et al., Nuclear Fusion **32** (1992) 1139.
[21] R. Van Nieuwenhove et al., Nucl. Fusion **31** (1991) 1770.
[22] R. Van Nieuwenhove et al., Nucl. Fusion **32** (1992) 1913.
[23] J. Sorensen et al., Nucl. Fusion **33** (1993) 915.
[24] J-M Noterdaeme et al., 16th Inter. Conf. on Fusion Energy (IAEA(Vienna), Montreal, 1997), p. 335.
[25] R.I. Pinsker et al., 11th Topical Conference on RF Power in Plasmas (AIP, Woodbury), p. 43.
[26] I.H. Hutchinson et al., Physics of Plasmas **1**, (1994) 1511.
[27] Y. Takase, S.N. Golovato, M. Porkolab, K. Bajwa, H. Becker, and D. Caldwell, 14th Symp. on Fusion Eng., San Diego, 1992, (IEEE, Piscataway, NJ, 1992), p. 118.
[28] S.J. Wukitch et al., Plasma Phys. Control. Fusion **46** (2004) 1479.
[29] L. L. Lao et al., Nucl Fusion **25** (1985) 1611.
[30] R.L. Boivin et al., *Rev. Sci. Instrum.* **70**, 260 (1999).
[31] J. A. Goetz et al., *J. Nucl. Mater.* **220**, 971 (1995).
[32] J.A. Goetz et al., Phys. Plasmas **3**, 1908 (1996).

[33] B. Lipschultz et al., Phys. Plasmas **13** (2006) 056117.
[34] R.A. Hulse, Nuclear Technology/Fusion **3** (1983) 259.
[35] J.E. Rice et al., Physics of Plasma **4** (1997) 1605.
[36] D.E. Post et al., Atomic Data and Nuclear Data Tables **20** (1977) 397.
[37] K.B. Fournier et al., Nuclear Fusion **37** (1997) 825.
[38] K.B. Fournier et al., Nuclear Fusion **38** (1998) 639.
[39] J. Winter, Plasma Phys. Control. Fusion **38** (1996) 1503.
[40] W.R. Wampler et al., J. Nuclear Mat. **266-269** (1999) 217.
[41] B. Lipschultz et al., this conference.
[42] S.J. Wukitch et al., Plasma Physics Control. Fusion **46** (2004) 1479.
[43] D. W. Swain et al., Nuclear Fusion **37** (1997) 1.
[44] D.A. D'Ippolito and J.R. Myra, Physics Plasmas **3** (1996) 420.

Figure Captions

Figure 1: Top view schematic showing the location of the antennas (D+E and J), limiters, and example of field lines mapped from each antenna. Note that these field lines map to toroidally distinct locations and the dashed circles mark the top of the outer divertor.

Figure 2: Poloidal cross section showing tile groups: (A) gusset; (B) limiter; (C) top of outer divertor; and (D) strike point. A set of poloidal projections of field lines are shown. Note that the field lines ending on the outer shelf intersect near the resonance position where impurities were controlled more effectively.

Figure 3: Comparison of stored energy and radiated power for control and test discharges. The red curve is representative of first discharge post boronization with D+E antenna and green is second discharge heated by J antenna. This discharge has nearly identical response as first and the second discharge heated by D+E shows its typical degradation and increase radiation.

Figure 4: Comparison of stored energy and radiated power for D+E series and J series of discharges. The dashed curves are for D+E and J are solid. The first discharge, shown in red, has good agreement between D+E and J. Green is the discharge identified as degraded performance. Note this is discharge #4 for J antenna compared to #2 for D+E. The blue line is discharge #3 for J.

Figure 5: J antenna with Faraday screen removed and septums installed.

Figure 6: Comparison of J antenna with Faraday screen removed and D+E antennas showing the degraded plasma performance.

Figure 7: Relative Cu density versus RF power for the J antenna with Faraday screen removed and D+E antennas.

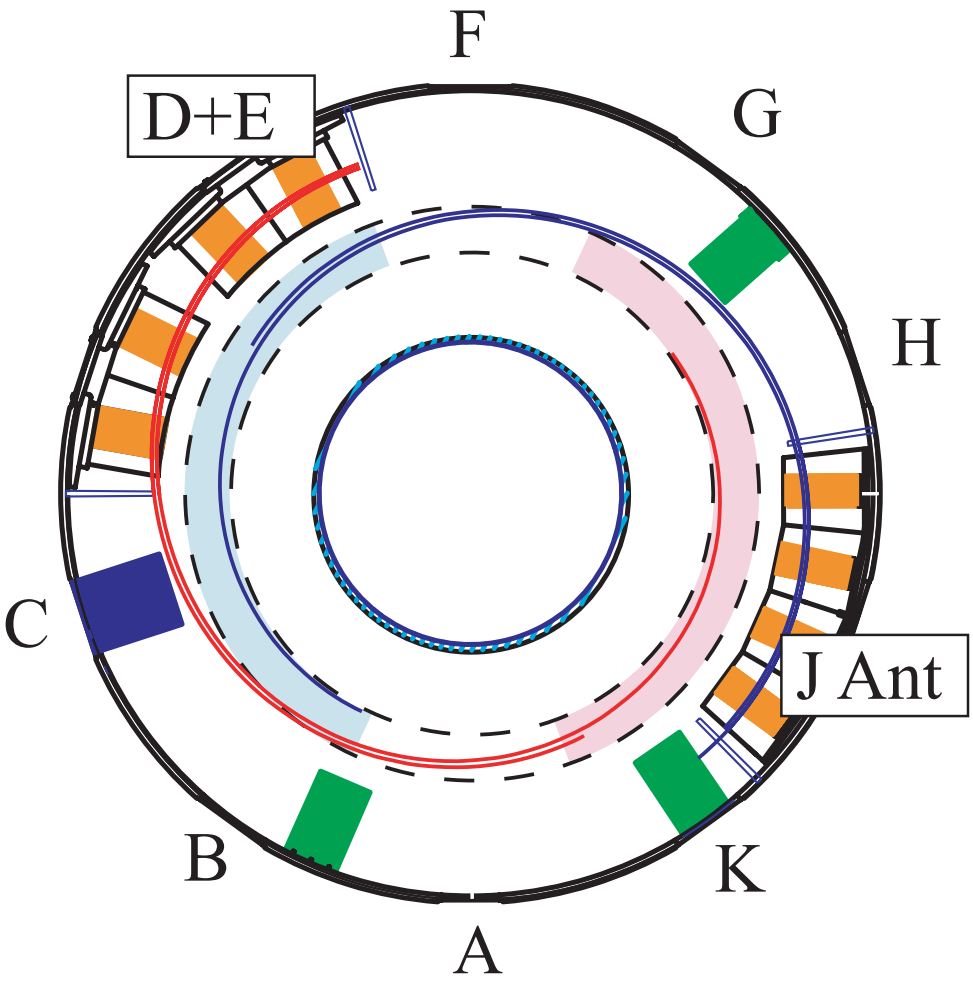

Figure 1

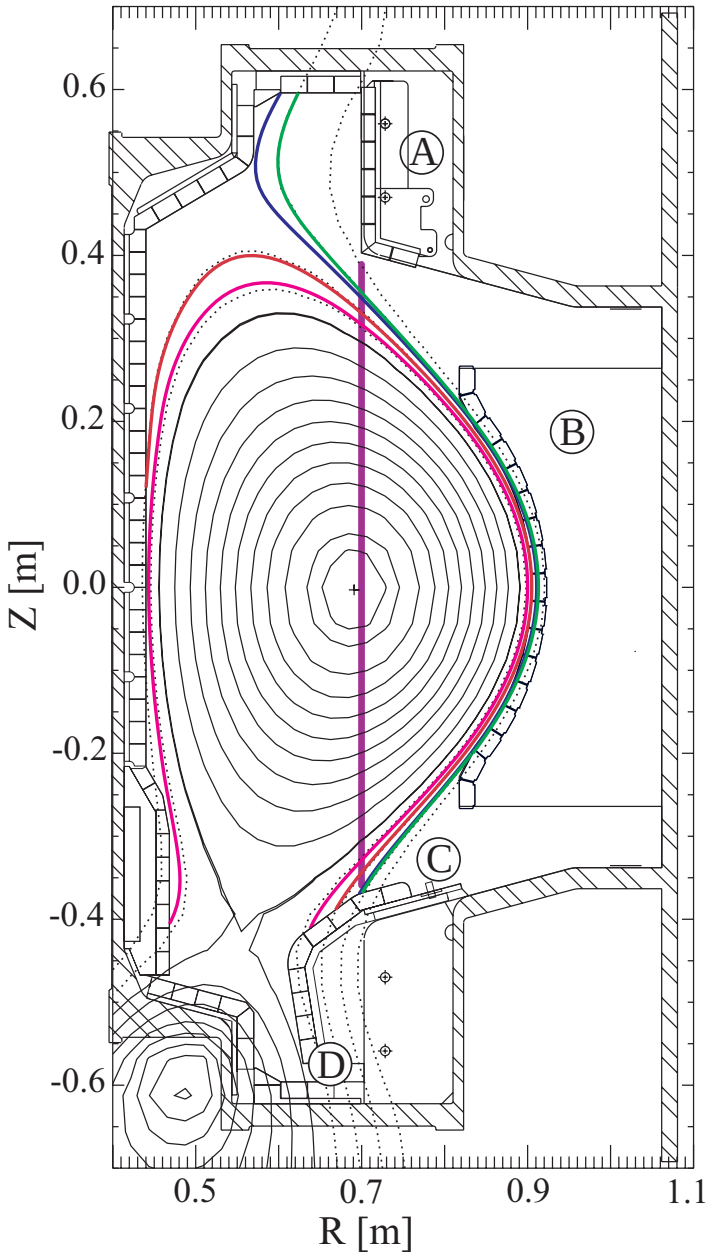

Figure 2

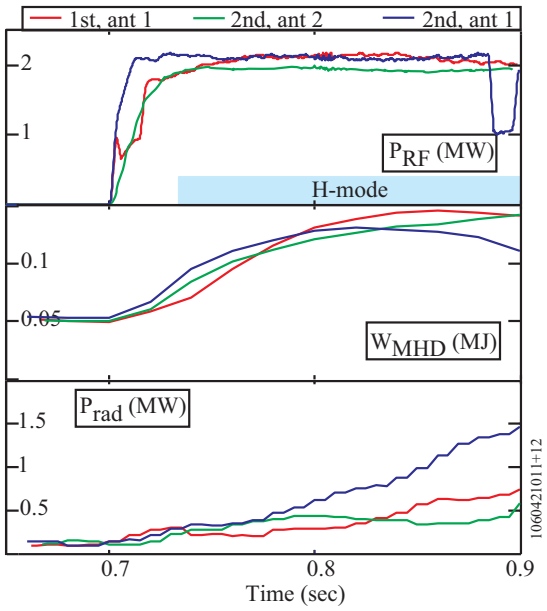
1st, ant 1
2nd, ant 2
2nd, ant 1
2
1
P_RF (MW)
H-mode
0.1
0.05
W_MHD (MJ)
P_rad (MW)
1.5
1
0.5
0.7
0.8
0.9
Time (sec)
1060421011+12

Figure 3

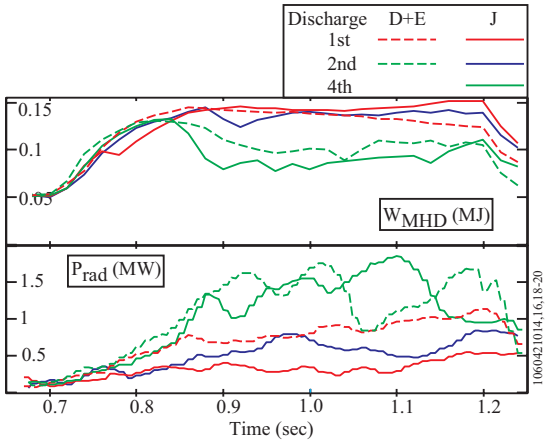
Discharge
D+E
J
1st
2nd
4th
0.15
0.1
0.05
W_MHD (MJ)
P_rad (MW)
1.5
1
0.5
0.7
0.8
0.9
1.0
1.1
1.2
Time (sec)
1060421014,16,18-20

Figure 4

Figure 5

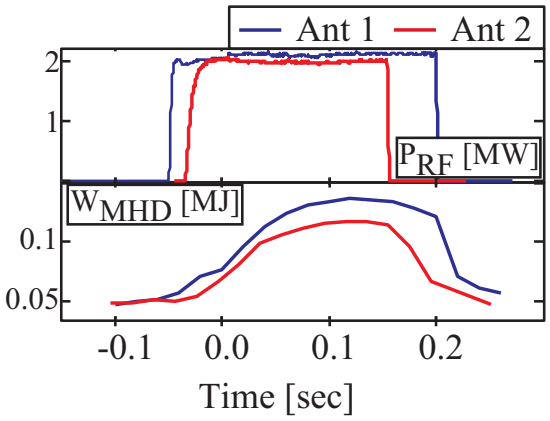

Figure 6

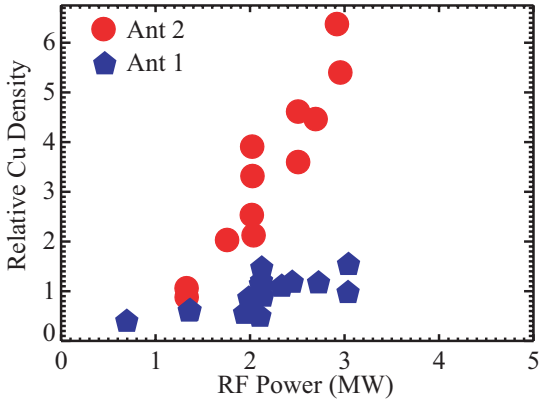

Figure 7